Chemical Science



EDGE ARTICLE

View Article Online
View Journal | View Issue



Cite this: Chem. Sci., 2023, 14, 8905

dll publication charges for this article have been paid for by the Royal Society of Chemistry

Received 23rd May 2023 Accepted 16th July 2023

DOI: 10.1039/d3sc02595k

rsc li/chemical-science

Chalcogen-doped, (seco)-hexabenzocoronenebased nanographenes: synthesis, properties, and chalcogen extrusion conversion†

Ranran Li,^a Bin Ma,^a Shengtao Li,^a Chongdao Lu [©] and Peng An [©] * ^{ab}

A series of chalcogen-doped nanographenes (NGs) and their oxides are described. Their molecular design is conceptually based on the insertion of different chalcogens into the hexa-peri-hexabenzocoronene (HBC) backbone. All the NGs adopt nonplanar conformations, which would show better solubility compared to planar HBC. Except for the oxygen-doped, saddle-shaped NG, the insertion of large chalcogens like sulfur and selenium leads to a seco-HBC-based, helical geometry. All the three-dimensional structures are unambiguously confirmed by single-crystal X-ray diffractometry. Their photophysical properties including UV-vis absorption, fluorescence, chiroptical, charge distribution, and orbital gaps are investigated experimentally or theoretically. The properties of each structure are significantly affected by the doped chalcogen and its related oxidative state. Notably, upon heating or adding an acid, the selenium-doped NG or its oxide undergoes a selenium extrusion reaction to afford seco-HBC or HBC quantitatively, which can be treated as precursors of hydrocarbon HBCs.

Introduction

Polycyclic aromatic hydrocarbons (PAHs) have fascinated chemists for a long time due to their wide utility in materials science,1 optoelectronic devices,2 biological probes,3 and supramolecular chemistry.4 To exploit three-dimensional aesthetic structures and modulate optoelectronic or photophysical properties, an increasing number of contorted polycyclic aromatic hydrocarbons (PAHs) or nanographenes (NGs) have been developed in the past decades.5 Such nonplanar PAHs or NGs have been constructed with a diversity of shapes, including bowls,6 saddles,7 helixes,8 belts,9 rings,10 and hybrid conformations11 by "bottom-up" strategies. Compared to their planar counterparts, nonplanar PAHs or NGs have shown intriguing properties including high solubility, different aggregation patterns, tunable optoelectronic properties, and specific supramolecular interactions.3a,12 Strategically, the introduction of main-group elements into hydrocarbon PAHs is another powerful method to not only modulate their threedimensional structures but tune their intrinsic properties including chemical reactivity, electronic energy gap, and photophysical behavior.13

As a planar NG unit, hexa-*peri*-hexabenzocoronene (HBC), a D_{6h} – symmetric planar π scaffold (Fig. 1a), and its derivative have been intensively studied. Owing to the nature of its planar structure, HBC generally exhibits low solubility and a high aggregation tendency in solvents, which commonly hampers its application, particularly in solution-based device fabrication. Thus, numerous efforts have been made to engineer the structure of HBC. For example, by incorporation of a non-hexagonal ring like a seven-, eight-, or nine-membered ring into the HBC skeleton, saddle-, or helical-,

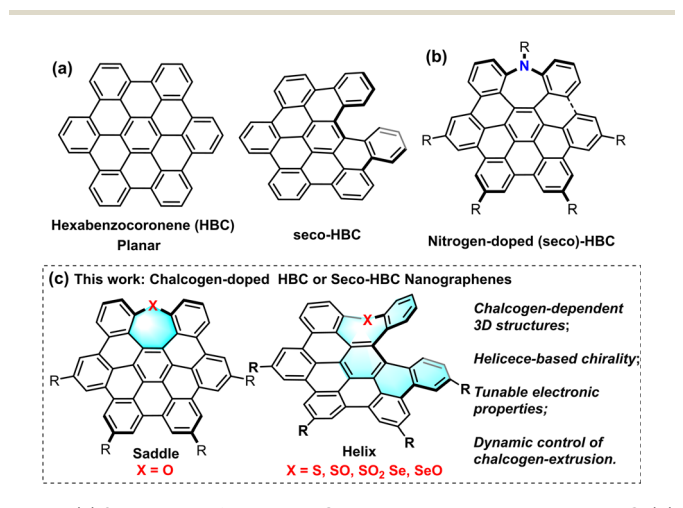


Fig. 1 (a) Structures of planar HBC and partially cyclized seco-HBC. (b) Structures of nitrogen-doped, (seco)-HBC-based NGs. (c) Insertion of chalcogens to design heteroatom-doped HBC or seco-HBCs.

[&]quot;School of Chemical Science and Technology, Yunnan University, Kunming 650091, P. R. China. E-mail: anp@ynu.edu.cn

^bKey Laboratory of Medicinal Chemistry for Natural Resource, Ministry of Education, Yunnan University, Kunming 650091, P. R. China

[†] Electronic supplementary information (ESI) available. CCDC 2238626–2238632. For ESI and crystallographic data in CIF or other electronic format see DOI: https://doi.org/10.1039/d3sc02595k

seco-HBC-based (Fig. 1a) structures were revealed, and these novel nonplanar structures exhibit distinct photophysical properties and aromaticity compared to the parent HBC. Recently, by insertion of nitrogen into the HBC backbone in the fjord region, our group reported nitrogen-doped HBC- or seco-HBC-based NGs^{7b,18} (Fig. 1b), and the optical properties can be mediated by introducing versatile substituents at the peripheral nitrogen. In this context, we focused our attention on the insertion of chalcogens into the HBC backbone. We envisioned that varied chalcogens in the new backbone of NGs would significantly affect the properties of the entire π -system in the following aspects: (1) specific atomic radii of doped chalcogens may lead to diverse three-dimensional structures; (2) distinct electronegativities and multiple oxidation states of chalcogens would be beneficial to sophisticatedly tune the electronic properties; (3) by means of the unique chalcogen-extrusion reaction,19 a specific reactivity toward atom-extrusion conversion would offer dynamic control of ring-reconstruction.

Thus, a series of chalcogen-doped NG analogs were designed and the influences of the doped chalcogens or oxidized chalcogens on the overall synthesis, structural geometry, electronic properties, and chalcogen extrusion reaction of the π -systems are demonstrated (Fig. 1c). Single-crystal X-ray analysis unequivocally reveals the saddle- and saddle-helix-shaped conformations of these novel chalcogen-doped NGs. The photophysical properties as well as the chiroptical properties of the helical, sulfur- and selenium-doped NGs were investigated. Meanwhile, thermal- or acid-induced chalcogen extrusion reactions for these NGs were studied, and the heteroatomdependent chalcogen-extrusion processes were observed. Particularly, the selenium-doped NGs exhibit controllable, fast, and quantitative selenium extrusion conversion to form HBC under acidic conditions at room temperature. For the first time, the saddle-helix precursors of HBC, with over 100-fold higher solubility than HBC, were identified. The details of these results will be elucidated in this article.

Results and discussion

Synthesis of chalcogen-doped nanographenes

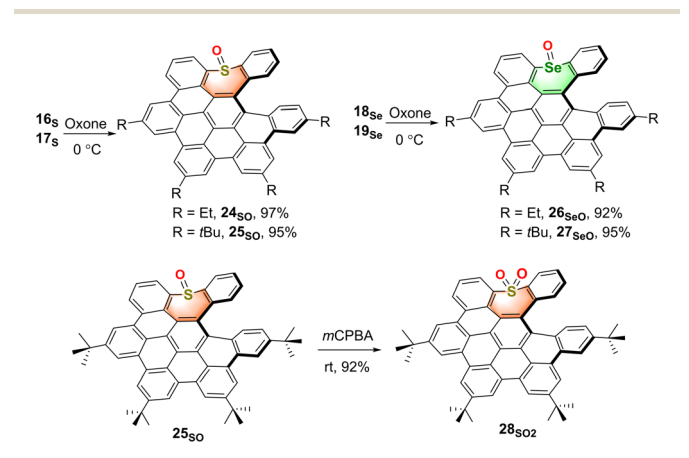
To obtain a series of chalcogen-doped NGs, we used a universal synthetic route to synthesize NGs with different alkyl side chains for single crystal cultivation (Scheme 1). In brief, the Diels-Alder reaction of dibenzo [b,f] oxepine (DBO) 1 with tetrabromothiophene-S,S-dioxide 2 in toluene followed by oxidative aromatization in the presence of 2,3-dichloro-5,6-dicyano-1,4benzoquinone (DDQ) afforded tetrabrominated aromatics 3 in 75% yield. Subsequently, fourfold Suzuki-Miyaura crosscoupling reactions of compound 3 with (4-ethylphenyl) boronic acid in the presence of 15 mol\% PdCl₂(CH₃CN)₂, 30 mol% SPhos and excess K₃PO₄ then furnished the hexaphenylbenzene 4 in 81% yield. The treatment of compound 4 with DDQ (10.0 equiv.) in the presence of triflic acid (13.0 equiv.) in DCM in a water-ice bath resulted in the fully fused oxa-NG 50 within 5 minutes in 65% yield with the formation of five new C-C bonds. For sulfur- or selenium-doped analogs, thiepine 8 and selenepine 9 were prepared in a two-step reaction with overall 58% and 24% yields respectively: the coppercatalyzed oxidative coupling of (2-formalphenyl) boronic acid with the sulfur or selenium followed by intramolecular McMurry olefin formation. Then Diels-Alder reactions of thiepine 8 and selenepine 9 with compound 2 followed by oxidative aromatization with DDO furnished compounds 10 and 11 in 90% and 56% yields respectively. Notably, a higher temperature (140 °C in xylene) and longer reaction time are needed for selenepine 9 compared to that for oxepine 1 and thiepine 8 in the Diels-Alder reaction (synthetic details in the ESI†). Then arylations for compounds 10 and 11 were performed using Suzuki-Miyaura cross-coupling conditions in the presence of

Scheme 1 Synthesis of oxygen-doped NG 5_O, sulfur-doped NGs 16_S, and 17_S, and selenium-doped NGs 18_{Se} and 19_{Se}.

Edge Article Chemical Science

15 mol% PdCl₂(CH₃CN)₂, 30 mol% SPhos, excess boronic acid, and K₃PO₄, affording hexaphenylbenzene 12-15 in 54-78% yields. When compounds 12-15 were subjected to Scholl reactions under the conditions of DDQ/CF₃SO₃H in DCM at 0 °C, the seco-HBC-based structures 16s, 17s, 18se, and 19se were obtained with the formation of four continuous C-C bonds. Instead of the fully cyclized saddle of oxygen-embedded NG, helical structures were formed for sulfur- and selenium-doped NGs presumably due to the large strain caused by atom size increasing. In any attempts of increasing the temperature, adding more equivalent reagents, or using other oxidative cyclization conditions, no fully fivefold cyclization product was observed (Scheme S6†). Meanwhile, the synthesis of telluriumdoped NGs was also investigated (Scheme S4†). In order to construct a tellurium-doped analog, we synthesized dibenzo[b,f] tellurepine 21 from dibromide 20 after failed attempts by using the same synthetic procedure as compounds 6 and 7 from boronic acid. Through two-fold lithium-halide exchange with *n*butyl lithium followed by tellurium insertion, compound 20 was successfully transformed to dibenzo[b,f]tellurepine 21 in 58% yield. The mono-tellurium-doped aromatics 21 was unambiguously confirmed by X-ray crystallography analysis.20 Subsequently, we subjected compound 21 to similar Diels-Alder reaction conditions by reacting with tetrabromide 2. Consequently, no tellurium-insertion product 22 was detected by gradually raising the heating temperature. Instead, we observed phenanthrene formed as the dominant product through tellurium extrusion of compound 21 upon heating to 140 °C, and some amount of tetrabromo 23 was observed when the heating temperature raised up to 180 °C. These results indicated that telluride 21 is prone to undergo a tellurium extrusion reaction prior to the Diels-Alder reaction, and compound 23 was most likely formed by [4 + 2] cycloaddition of phenanthrene and compound 2. Structure 23 was also confirmed by X-ray crystallography analysis.20 Hence, the tellurium extrusion process suggested a higher possibility of heteroatom-extrusion by doping a larger-size chalcogen.

With the sulfur- and selenium-doped NGs in hand, their oxidative analogs were prepared (Scheme 2). The selective oxidation of sulfur-NGs 16_S and 17_S and selenium-NGs 18_{Se} and



Scheme 2 Synthesis of oxidative derivatives of S-, Se-doped NGs.

19_{Se} was performed by treating them with oxone at 0 °C for 2 hours to afford the corresponding mono-oxides 24_{so} and 25_{so}, and 26_{SeO} and 27_{SeO} in nearly quantitative conversion. Meanwhile, the S,S-dioxide 28502 was obtained by oxidation of compound 25_{so} at room temperature in the presence of an excess amount of meta-chloroperoxybenzoic acid (m-CPBA), while 27_{seo} cannot be oxidized under these conditions. Due to the highly distorted skeletons, all the chalcogen-doped NGs as well as the corresponding oxides show good solubility in organic solvents; therefore, they could be unequivocally confirmed by means of 1H- and 13C NMR spectroscopy (Fig. S29-S50†) and high-resolution mass spectrometry (see the ESI \dagger). Meanwhile, the seco-HBC-type molecules including 16_s, 18_{se}, and 24_{so} were further characterized by 2D ¹H-¹H ROESY and COSY (Fig. S1-S3†).

Structural analysis of NGs

We next try to grow single crystals for all the NGs with different alkyl chains, and as a result, single crystals of 50, 17s, 18se, and 24_{SO} suitable for X-ray diffraction analysis were obtained by slowly evaporating their solutions at room temperature (Tables S1 and S2†).20 As shown in Fig. 2a-d, all the molecular backbones are distorted due to the incorporation of a heteroatomdoped, seven-membered ring. All the seven-membered rings exhibit different degrees of antiaromaticity suggested by nucleus-independent chemical shift (NICS)21 by DFT calculations at the B3LYP/6-311+G(d,p) level of theory (Fig. S27†). Positive NICS (0) values between 2.79 and 6.49 were observed for all chalcogen-doped, seven-membered rings. The localized orbital locator (LOL)- π electron distribution calculation indicated that the electrons were localized on the seven hexagonal rings with strong π -conjugation (Fig. S27†). In detail, the X-ray crystallographic analysis of 50 reveals a saddle-shaped, negatively curved structure in which the oxygen atom protrudes from the π surface. Such a distorted conformation resembles that of a previously reported N-Me doped analog.7b The depths of the saddle, defined as the perpendicular distance from the centre of ring A to the line across C14 and C3 is 0.91 A (Fig. 2e), slightly shallower than the N-Me doped analogue. Meanwhile, the structures of 17s, 18se, and 24so exhibited saddle-helix geometry with a protruding chalcogen out of the π surface (Fig. 2b-d). The end-to-end dihedral angle of [5]helicene in NG 17s defined as the angle formed by the two benzene rings located at its terminal edges is 71.4°, and the torsion angle (C8-C14-C12-C38) is 34.9° (Fig. 2b). Meanwhile the dihedral angle and torsion angle in NG 18_{Se} are 73.0° and 32.2° (C5-C4-C3-C2) respectively (Fig. 2c). Longer Se1-C1 (1.917 Å) and Se1-C35 (1.920 Å) bonds in 18_{Se} were observed compared to C-S bonds (1.766 and 1.778 Å) in 17_s due to the larger atomic radii of selenium. Both helicenes 17s and 18se exhibited a larger end-toend dihedral angle and torsion angle than the nitrogen-doped analogs (64.4° and 31.1° respectively)^{18b} due to the increased atom size of sulfur and selenium. As helicenes, the crystallography of both 17s and 18se, shown in Fig. 2f as a representative example, displays P/M enantiomers in single crystal structures (Fig. S5 and S6†). The S-oxide 24_{so} was also unequivocally

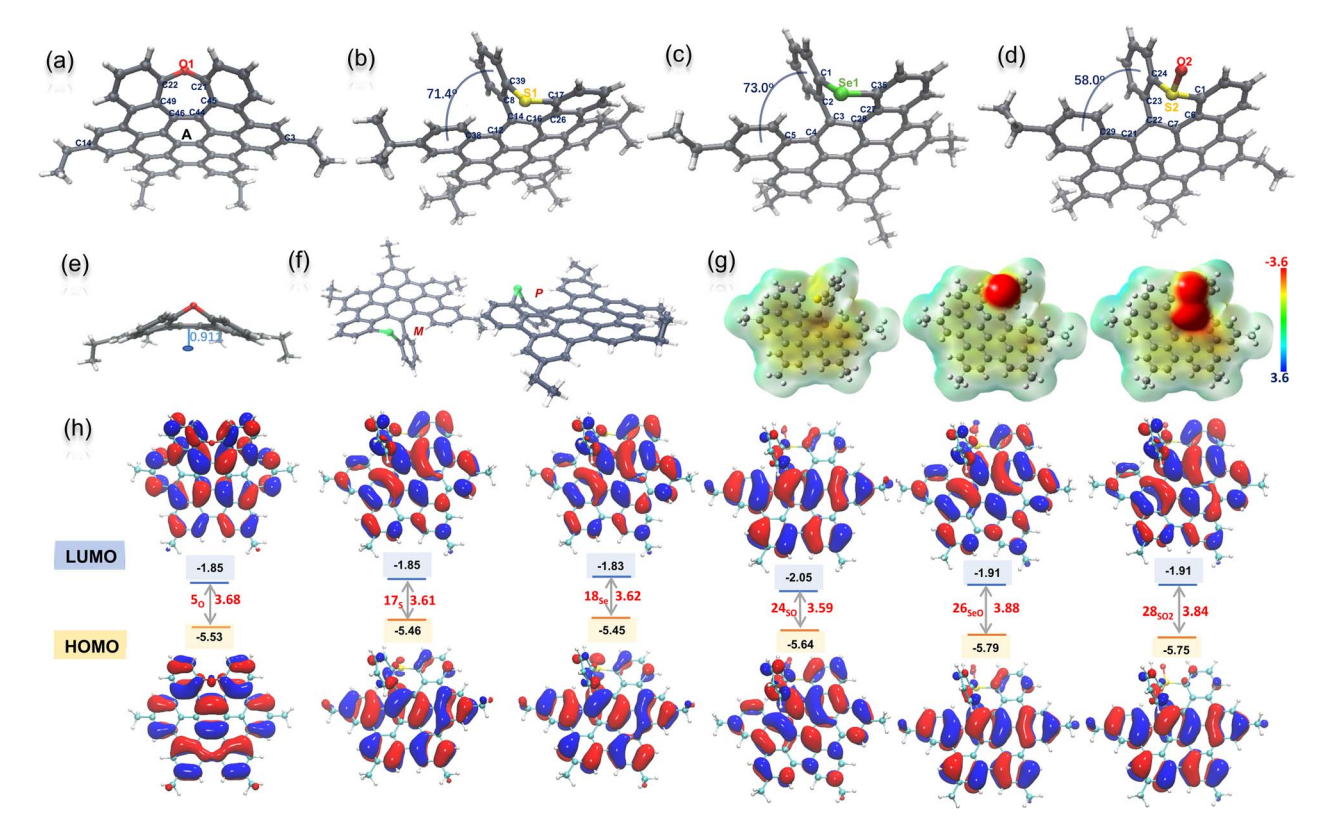


Fig. 2 X-ray crystallographic structures of $5_{\rm O}$ (a), $17_{\rm S}$ (b), $18_{\rm Se}$ (c), and $24_{\rm SO}$ (d) with 50% probability of thermal ellipsoids. Side view of the saddle-shaped NG $5_{\rm O}$ with the saddle-depth marked (e) and a pair of enantiomers shown in the single crystal $18_{\rm Se}$ (f). Electrostatic potential (ESP) maps and the energy colour bar (a.u.) of S-, SO-, and SO₂-doped NGs (g), in which the alkyl chains were replaced by methyl groups. TD-DFT calculation of HOMO and LUMO orbitals with energies (eV) of $5_{\rm O}$, $17_{\rm S}$, $18_{\rm Se}$, $24_{\rm SO}$, $26_{\rm SeO}$, and $28_{\rm SO2}$ at the PBE0/6-311G(d,p) level of theory (h). The alkyl chains were replaced by methyl groups.

confirmed by its X-ray structure (Fig. 2d). The formation of the SO bond decreased the end-to-end dihedral angle (58° in 24_{SO}) and torsion angle (29.8°, C23-C22-C21-C29). Due to the electronegativity of sulfoxide, the intermolecular hydrogen bond interaction between sulfoxide and dichloromethane was observed in the crystal packing besides the π - π stacking (Fig. S7†). The electron-static potential (ESP) map of 17_s, 24_{so}, and 28_{SO2} obtained through DFT calculations at the CAM-B3LYP/6-31+(d,p) level of theory (Fig. 2g) clearly showed the influence of different sulfur-oxidation states on the charge of the NG molecules. As expected, the electrons were distributed almost evenly on the surface of sulfur-doped NG 17s, and aggregated at the oxygen once the sulfur was oxidized in 24so, and 28_{SO2}. The HOMO and LUMO orbitals²² of seco-HBC-based NGs 17_S , 19_{Se} , 24_{SO} , 26_{SeO} , and 28_{SO2} calculated at the PBE0/6-311G(d,p) level do not differ a lot from each other: each HOMO is found to be delocalized on the entire molecule, while the LUMOs are delocalized on the coplanar benzenoid rings (Fig. 2h).

Photophysical and electrochemical properties

The optical properties of chalcogen-doped NGs were investigated by UV-vis absorption and fluorescence spectroscopy. The UV-vis spectra of $5_{\rm O}$, $17_{\rm S}$, $19_{\rm Se}$, $25_{\rm SO}$, and $27_{\rm SeO}$ in DCM show that

the absorption maxima are nearly identical (351-353 nm) together with multiple shoulder peaks, while sulfone 28₅₀₂ exhibits a red-shifted absorption band with the maximum peak at 360 nm (Fig. 3a). The weak absorption peaks of 50, 24so, and 26_{seO} with ethyl substituents at approximately 450 nm were observed rather than the tert-butyl substituted analogs probably due to the formation of an exciplex by intermolecular π - π interaction (Fig. S8†). To obtain insights into the origin of the absorptions, we conducted time-dependent density-functional theory (TD-DFT) (Fig. S28, Tables S10-S15†). The DFT calculations indicated that the lower-energy bands at around 430 and 400 nm are mainly contributed by the HOMO-LUMO transition. The high-energy bands at approximately 375 and 350 nm can be assigned to either HOMO-LUMO+1 or HOMO-1-LUMO and HOMO-1-LUMO+1 respectively, which exhibit larger oscillator strength. The fluorescence maximum of these NGs is similarly located at around 475 nm with shoulder emission peaks for 5_{01} and a bathochromic-shifted peak at 490 nm for 28502 was observed (Fig. 3b). These compounds exhibit a large Stokes shift of 120 nm (over 7200 cm⁻¹). Meanwhile, these chalcogen-doped NGs exhibit fluorescence intensity that depends on the doped heteroatoms and their oxidative state. With a similar helical conformation, 17s doped with sulfur exhibited 10-fold higher fluorescence intensity and nearly 20-fold higher fluorescence quantum yield (Table S3†) than the selenium-doped analog

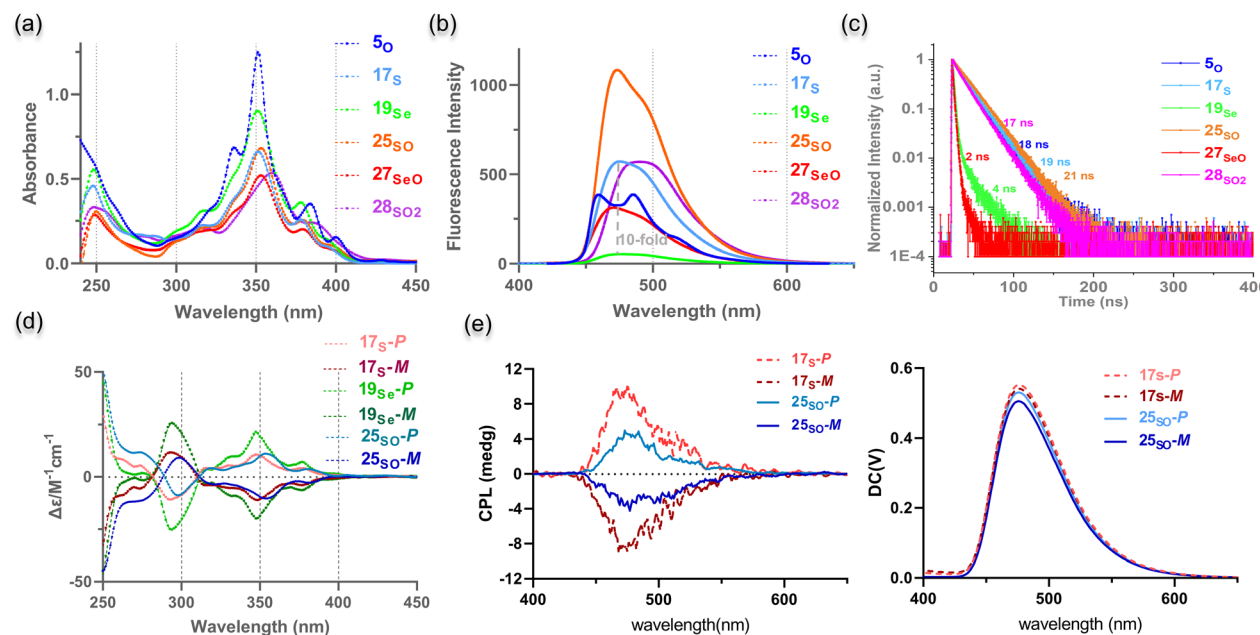


Fig. 3 Photophysical and chiroptical properties of chalcogen-doped NGs. (a) UV-vis absorption spectra, (b) fluorescence emission spectra, and (c) fluorescence decay profiles of $\mathbf{5}_O$, $\mathbf{17}_S$, $\mathbf{19}_{Se}$, $\mathbf{25}_{SO}$, $\mathbf{27}_{SeO}$, and $\mathbf{28}_{SO2}$. The spectra were collected in DCM solution with 5 μ M concentration and $\lambda_{exc.}=350$ nm for fluorescence excitation. (d) CD spectra of enantiomeric $\mathbf{17}_S$ -P and $\mathbf{17}_S$ -M, enantiomeric $\mathbf{19}_{Se}$ -P and $\mathbf{19}_{Se}$ -M, and enantiomeric $\mathbf{25}_{SO}$ -P and $\mathbf{25}_{SO}$ -M in hexane. (e) CPL and direct current (DC) spectra of $\mathbf{17}_S$ -P/ $\mathbf{17}_S$ -M and $\mathbf{25}_{SO}$ -P/ $\mathbf{25}_{SO}$ -M in dichloromethane ($\lambda_{exc.}=350$ nm, the measurement was carried out in air).

19_{Se}. The fluorescence efficiency of NGs can be significantly enhanced by changing the doping heteroatoms S or Se to *S*-oxide or Se-oxide (**17**_S νs. **25**_{SO}; **19**_{Se} νs. **26**_{SeO}, Fig. 3b, Table S3†). As a result, the *S*-oxide **25**_{SO} was highly fluorescent with the highest fluorescence quantum yield of 0.30, which is significantly higher than that of the corresponding HBC **30**_{HBC} and *seco*-HBC **29**_{seco-HBC} (Table S3†). Notably, the difference in the magnitude of the fluorescence decay was observed by doping different heteroatoms. As shown in Fig. 3c, the oxygen- and sulfur-doped candidates **5**_O, **17**_S, **25**_{SO}, and **28**_{SO2} exhibit very close decay rates with fluorescence lifetimes over **17** ns, whereas, for selenium-doped compounds **19**_{Se} and **27**_{SeO}, the fluorescence lifetimes are less than 4 ns. Electrochemical properties were investigated by cyclic voltammetry in CH₂Cl₂ in the presence of Bu₄NPF₆ as a supporting electrolyte (Fig. S11†).

Notably, the redox properties can be modulated by controlling the oxidative states of the doped chalcogens. The oxidized structures 25_{SO} , 27_{SeO} , and 28_{SO2} show more oxidation waves than their reduced analogs 17_{S} and 19_{Se} .

Chiroptical properties and determination of the racemization barrier

Helicene-based NGs have triggered much interest in the past decades due to their intrinsic chirality. We attempt to resolve the two sets of enantiomers for both $17_{\rm S}$ and $19_{\rm Se}$ and study their chiroptical properties. The enantiomers of $17_{\rm S}$ and $19_{\rm Se}$ were successfully separated by chiral high-performance liquid chromatography (HPLC) at 25–30 °C with ethanol as the mobile phase (Fig. S12 and S13†). The electronic circular dichroism (ECD) spectra of the enantiomers of $17_{\rm S}$ and $19_{\rm Se}$ in hexane

demonstrated a perfect mirror image relationship with multiple opposite Cotton effects in the UV/vis region from 200 to 450 nm (Fig. 3d). Due to the homologous chiral structures, similar profiles of enantiomers from 17_S and 19_{Se} were displayed. Each enantiomer of 17_S or 19_{Se} was confirmed by comparing each ECD spectrum with the calculated spectrum (Fig. S26†). Since sulfoxide 25_{SO} shows high emission efficiency, we prepared the optically pure enantiomers 25_{SO}-P/25_{SO}-M by oxidation of enantiomers 17_S-P and 17_S-M (Fig. S14†), and the ECD spectra of 25_{SO}-P/25_{SO}-M indicated a perfect enantiomer relationship (Fig. 3d). Next, we carried out circularly polarized luminescence (CPL) measurements for each enantiomer. The CPL spectra of 17_S-P/17_S-M and 25_{SO}-P/25_{SO}-M exhibited a mirror-imaging relationship in dichloromethane under ambient conditions (Fig. 3e), which suggested that 17_S and 25_{SO} show CPL activity.

The luminescence dissymmetry ratio (g_{lum}), evaluating the degree of CPL, was determined to be 1.1×10^{-3} and 5.6×10^{-4} for $17_{\rm S}$ and $25_{\rm SO}$ respectively at 480 nm (Fig. S15†). Due to the low fluorescence quantum yield ($\Phi_{\rm F}$ < 0.01), the CPL of $19_{\rm Se}$ -P and $19_{\rm Se}$ -M was feeble to be detected. Meanwhile, due to the high extinction coefficient and $\Phi_{\rm F}$, the enantiomers of $17_{\rm S}$ and $25_{\rm SO}$ exhibit $B_{\rm CPL}$ up to 13 M⁻¹ cm⁻¹ and 12 M⁻¹ cm⁻¹ respectively. The successful resolution of two enantiomers of $17_{\rm S}$ or $19_{\rm Se}$ indicated relatively high enantiomerization barriers for both helicenes.

To experientially determine the isomerization barrier (ΔG^{\ddagger}), thermal racemization of optically pure 17_{S} -P was performed followed by chiral HPLC analysis (Fig. S16†). HPLC traces of the samples after heating at 100 °C exhibited a clean transformation from the 17_{S} -P to the 17_{S} -M isomer. The half-life ($\tau_{1/2}$)

Chemical Science

for loss of enantiomeric excess was determined to be 5.5 hours at 100 °C. It gives a racemization barrier ΔG^{\ddagger} (373 K) of 29.6 kcal mol⁻¹ using the Eyring equation, which demonstrated a relatively stable helicene enantiomer and comparable with reported [5]helicene containing NGs.24 In addition, thermal racemization of optically pure 19_{Se}-P was performed similarly. However, 19_{Se}-P stayed stable after heating at 100 °C for hours, which suggested a higher isomerization barrier of 19se than that of 17s. Interestingly, the selenium-extrusion reaction was observed together with enantiomerization when the heating temperature was raised to 130 °C (Fig. S17†). Nevertheless, excluding other chemical reactivity, the racemization barrier ΔG^{\ddagger} of $\mathbf{19}_{\mathbf{Se}}$ was evaluated to be 31.2 kcal mol⁻¹ at 403 K.

Chalcogen-extrusion processes

After getting a hint from the observation of the seleniumextrusion process during the synthesis, we then investigated the chalcogen-extrusion reactions of these heteroatom-doped NGs. Several organosulfur compounds are susceptible to undergoing photo- or thermal-induced sulfur extrusion reactions.25 Initially, we examined whether the extrusion reactions could be triggered by UV light. Each compound was treated in DCM solution under an atmosphere of N2, followed by photoirradiation with 254 or 365 nm UV light. Unfortunately, no distinct change was observed for all the NGs upon irradiation for a short period of time (<10 min) and compounds gradually degraded over a long time. Alternatively, we performed the thermal chalcogen extrusion for compounds 50, 17s, 19se, 25so, 27_{SeO}, and 28_{SO2} (Fig. 4a). The experiments were conducted by heating milligrams of solid of each sample in an oven for a specific time, and monitoring the changes in the absorption spectra after re-dissolving the preheated sample in DCM. To our delight, for selenium-doped candidates, 19se and 27seo, identical de-selenium products were detected by observing the same absorption profiles formed after heating at 200 °C for only 5 min. These new species were confirmed as selenium-extrusion product 29_{seco-HBC} in comparison with the UV-absorption of standard product 29seco-HBC (Fig. 4be). The HPLC analyses of the brown samples formed upon heating (Fig. 4b, inset) indicated a quantitative formation of 29_{seco-HBC} (Fig. S20 and S21†). In contrast, sulfur 17_s and sulfone 28_{SO2} as well as the oxygendoped saddle 50 showed no change in the absorption spectra upon heating up to 250 °C for 2 hours, which suggests relatively thermally stable structures (Fig. 4c, f, and S18†). Meanwhile, sulfoxide 25_{SO} exhibited an inert sulfur extrusion process by heating over 250 °C compared to selenium-doped analogs (Fig. 4d and S19†). These results suggested the accessibility and rate of chalcogen extrusion reaction are highly dependent on the sort and oxidative state of the embedded chalcogens.

The HBC reveals wide application in materials science but is detrimental to the fabrication of material devices due to aggregation-caused low solubility. Apparently, having a soluble precursor of HBC would significantly facilitate the material fabrication of HBC. We envisioned whether HBC structures be obtained by spontaneous oxidative cyclodehydrogenation of the chalcogen-extrusion products. By screening commonly used acids like acetic acid, HCl, and trifluoroacetic acid, it was found that selenium oxide 27seo could slowly convert to 30_{HBC} in a trifluoroacetic acid/DCM (1/2, v/v) solution (Fig. 5a) and the formation of target product 30_{HBC} was unequivocally confirmed by X-ray crystallography (Fig. 5b, Scheme S5†).20 As monitored by UV-vis absorption (Fig. 5c), through selenium extrusion and spontaneous oxidation in air, the characteristic peak of 27_{SeO} at 353 nm gradually shifted to

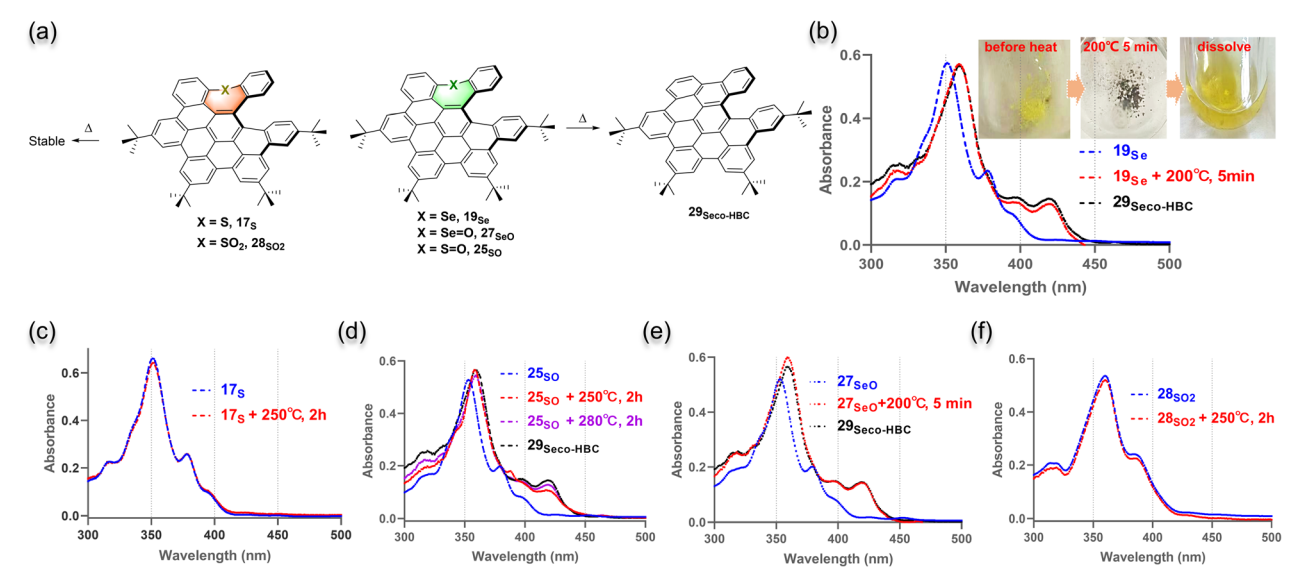


Fig. 4 (a) Chalcogen extrusion reactions of S-, Se-doped NGs. UV-vis absorption spectra of 19_{Se} (b), 17_{S} (c), 25_{SO} (d), 27_{SeO} (e), and 28_{SO2} (f) before and after heating. The spectra were collected by dissolving the solid (before and after heating) in DCM and the heating time of each compound was shown in the corresponding spectrum. For comparison, the UV-vis spectra of the chalcogen-extrusion product 29_{seco-HBC} were shown together with 19_{se} (b), 25_{so} (d), and 27_{seo} (e). The inset in (b) shows the photographic images of the 19_{se} solid before and after heating, and the dissolved brown heated solid in DCM.

Edge Article Chemical Science

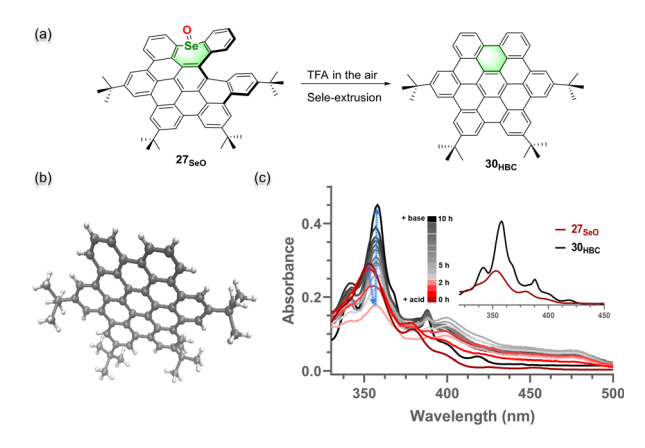


Fig. 5 (a) Acid-catalyzed HBC formation from HBC precursor selenium-doped NG 27_{SeO} . (b) X-ray crystallographic structure of 30_{HBC} with 50% probability of thermal ellipsoids. (c) Changes in the UV-vis absorption spectra of 27_{SeO} upon dissolving it in trifluoroacetic acid/ DCM (1/2, v/v) with 3.3 µM concentration under ambient conditions.

358 nm over 20 hours in the trifluoroacetic acid/DCM (1/2, v/v) solution, and the absorption spectrum after a 20 hour reaction was almost identical to that of 30_{HBC} , whereas the other NGs were stable under these conditions (Fig. S23†). Together with the HPLC analyses (Fig. S22†), a nearly quantitative conversion was obtained for 27_{seo} . Moreover, this transformation could be accelerated by the addition of stronger acid methanesulfonic acid instead of trifluoroacetic acid (Fig. S24†). To evaluate the difference in soluble properties between HBC and this precursor, we measured the solubility of 27_{SeO} and 30_{HBC} in dichloromethane and ethanol (Fig. S25†). The precursor 27_{SeO} exhibits more than 100-fold higher solubility in either dichloromethane or polar solvent ethanol.

Conclusions

We have developed a new class of chalcogen-doped NGs, in which a chalcogen is conceptually embedded into the HBC or seco-HBC backbone in the fjord region. As a eesult of the size of chalcogens, two types of structures were obtained toward the final step of the oxidative ring closure reaction: the oxygendoped saddle and the sulfur- or selenium-doped helix. The saddle and helical three-dimensional structures of the chalcogen-doped NGs and the sulfur-oxide were revealed by single-crystal X-ray diffraction analysis, and both P- and Menantiomers of helicene enantiomers cocrystallize in a single crystal. Enantiomers of sulfur- and selenium-doped helical NGs were isolated by chiral HPLC. The chiroptical properties including ECD and CPL were investigated and the sulfurembedded NG exhibited CPL activity with a g_{lum} of 1.1 \times 10⁻³ at 480 nm and $B_{\rm CPL}$ of 13 M⁻¹ cm⁻¹. The racemic barriers of S-NG and Se-NG were determined to be 29.6 and 31.2 kcal mol⁻¹ respectively by HPLC-based thermal isomerization. The experimental and computational study including UV-vis absorption, fluorescence emission, efficiency, decay, HOMO-LUMO gaps, and charge distribution indicated that the chalcogen and its oxidative state in the NG significantly affect the electronic

properties. The stability measurements of these NGs upon heating suggested that the Se-doped NG and its oxide undergo quantitative selenium-extrusion reactions, which offers dynamic control of the structural reconstruction. Notably, the highly distorted helical Se-oxide NG can transform to planar HBC under acidic conditions. The planar HBC generally exhibits low solubility and a high aggregation tendency in solvents. This HBS precursor would significantly facilitate the application of HBC in material fabrication.

Data availability

The full experimental details, synthetic procedures, characterization data, HPLC traces, UV-vis, fluorescence, IR and NMR spectra, computational details, and supplementary discussions associated with this article are provided in the ESI.†

Author contributions

Ranran Li performed most of the synthesis work and property studies. Bin Ma started the initial synthesis of compound 50. Shengtao Li helped with NMR, HPLC, and photophysical property measurements. P. An performed the DFT calculation and conceived the concept. P. An and C. Lu prepared and revised the manuscript. All the authors analyzed and interpreted the results.

Conflicts of interest

There are no conflicts to declare.

Acknowledgements

We are grateful for the financial support provided by the National Natural Science Foundation of China (21901226 and 22061046). We thank the advanced analysis and measurement center of Yunnan University for assistance with instrumentation. Particularly, we thank Dr Jie Zhou from the Advanced Analysis and Measurement Center of Yunnan University for the X-ray analysis.

Notes and references

- 1 (a) C. Wang, H. Dong, W. Hu, Y. Liu and D. Zhu, Chem. Rev., 2012, 112, 2208-2267; (b) K. S. Novoselov, V. I. Falko, L. Colombo, P. R. Gellert, M. G. Schwab and K. Kim, Nature, 2012, 490, 192-200; (c) L. Zhang, Y. Cao, N. S. Colella, Y. Liang, J.-L. Brédas, K. N. Houk and A. L. Briseno, Acc. Chem. Res., 2015, 48, 500-509; (d) X.-Y. Wang, X. Yao and K. Müllen, Sci. China: Chem., 2019, 62, 1099-1144.
- 2 (a) Q. Miao, Adv. Mater., 2014, 26, 5541-5549; (b) N. Bachar, L. Liberman, F. Muallem, X. Feng, K. Müllen and H. Haick, ACS Appl. Mater. Interfaces, 2013, 5, 11641-11653; (c) V. B. R. Pedersen, S. K. Pedersen, Z. Jin, N. Kofod, B. W. Laursen, G. V. Baryshnikov, C. Nuckolls and M. Pittelkow, Angew. Chem., Int. Ed., 2022, 61, e202212293.

(a) H.-A. Lin, Y. Sato, Y. Segawa, T. Nishihara, N. Sugimoto,
 L. T. Scott, T. Higashiyama and K. Itami, Angew. Chem., Int. Ed.,
 2018, 57, 2874–2878; (b) Q.-Q. Li, Y. Hamamoto,
 G. Kwek, B. Xing, Y. Li and S. Ito, Angew. Chem., Int. Ed.,
 2022, 61, e202112638; (c) Y.-F. Wu, S.-W. Ying, L.-Y. Su,
 J.-J. Du, L. Zhang, B.-W. Chen, H.-R. Tian, H. Xu,
 M.-L. Zhang, X. Yan, Q. Zhang, S.-Y. Xie and L.-S. Zheng, J.
 Am. Chem. Soc., 2022, 144, 10736–10742.

Chemical Science

- 4 (a) T. Kawase and H. Kurata, Chem. Rev., 2006, 106, 5250–5273; (b) J. Wu, W. Pisula and K. Müllen, Chem. Rev., 2007, 107, 718–747; (c) W. Pisula, X. Feng and K. Müllen, Chem. Mater., 2011, 23, 554–567; (d) D. Bialas, E. Kirchner, M. I. S. Röhr and F. Würthner, J. Am. Chem. Soc., 2021, 143, 4500–4518; (e) N. Zhang, L. Yang, W. Li, J. Zhu, K. Chi, D. Chang, Y. Qiao, T. Wang, Y. Zhao, X. Lu and Y. Liu, J. Am. Chem. Soc., 2022, 144, 21521–21529; (f) L. Chai, Y.-Y. Ju, J.-F. Xing, X.-H. Ma, X.-J. Zhao and Y.-Z. Tan, Angew. Chem., Int. Ed., 2022, 61, e202210268; (g) S. Zank, J. M. Fernández-García, A. J. Stasyuk, A. A. Voityuk, M. Krug, M. Solà, D. M. Guldi and N. Martín, Angew. Chem., Int. Ed., 2022, 61, e202112834.
- 5 (a) M. Rickhaus, M. Mayor and M. Juríček, Chem. Soc. Rev., 2017, 46, 1643-1660; (b) S. H. Pun and Q. Miao, Acc. Chem. Res., 2018, 51, 1630-1642; (c) Y. Segawa, H. Ito and K. Itami, Nat. Rev. Mater., 2016, 1, 15002; M. A. Majewski and M. Stepień, Angew. Chem., Int. Ed., 2019, 58, 86-116; (e) I. R. Márquez, S. Castro-Fernández, A. Millán and A. G. Campaňa, Chem. Commun., 2018, 54, 6705-6718; (f) S. R. Peurifoy, T. J. Sisto, F. Ng, M. L. Steigerwald, R. Chen and C. Nuckolls, Chem. Rec., 2019, 19, 1050-1061; (g) Y.-T. Wu and J. S. Siegel, Chem. Rev., 2006, 106, 4843-4867; (h) R. A. Pascal, Chem. Rev., 2006, **106**, 4809–4819; (i) A. Bedi and O. Godron, Acc. Chem. Res., 2019, 52, 2482-2490; (j) M. C. Stuparu, Acc. Chem. Res., 2021, 54, 2858–2870; (k) J. Wang, X. Zhang, H. Jia, S. Wang and P. Du, Acc. Chem. Res., 2021, 54, 4178-4190; (1) M. Grzybowski, B. Sadowski, H. Butenschön and D. T. Gryko, Angew. Chem., Int. Ed., 2020, 59, 2998-3027.
- 6 (a) M. Krzeszewski, Ł. Dobrzycki, A. L. Sobolewski, M. K. Cyrański and D. T. Gryko, Angew. Chem., Int. Ed., 2021, 60, 14998–15005; (b) H. Yokoi, Y. Hiraoka, S. Hiroto, D. Sakamaki, S. Seki and H. Shinokubo, Nat. Commun., 2015, 6, 8215.
- 7 (a) J. Luo, X. Xu, R. Mao and Q. Miao, J. Am. Chem. Soc., 2012, 134, 13796–13803; (b) P. An, R. Li, B. Ma, R.-Y. He, Y.-K. Zhang, M.-J. Xiao and B. Zhang, Angew. Chem., Int. Ed., 2021, 60, 24478–24483; (c) T. Kirschbaum, F. Rominger and M. Mastalerz, Angew. Chem., Int. Ed., 2020, 59, 270–274; (d) T. Kirschbaum, F. Rominger and M. Mastalerz, Chem.–Eur. J., 2020, 26, 14560–14564; (e) I. R. Márquez, N. Fuentes, C. M. Cruz, V. Puente-Muñoz, L. Sotorrios, M. L. Marcos, D. Choquesillo-Lazarte, B. Biel, L. Crovetto, E. Gómez-Bengoa, M. T. González, R. Martin, J. M. Cuerva and A. G. Campaña, Chem. Sci., 2017, 8, 1068–1074.
- 8 (a) N. Ogawa, Y. Yamaoka, H. Takikawa, K.-I. Yamada and K. Takasu, J. Am. Chem. Soc., 2020, 142, 13322–13327; (b)
 M. M. Martin, F. Hampel and N. Jux, Chem.–Eur. J., 2020,

- **26**, 10210–10212; (*c*) J. Ma, Y. Fu, E. Dmitrieva, F. Liu, H. Komber, F. Hennersdorf, A. A. Popov, J. J. Weigand, J. Liu and X. Feng, *Angew. Chem., Int. Ed.*, 2020, **59**, 5637–5642; (*d*) X.-Y. Chen, J.-K. Li and X.-Y. Wang, *Chinese J. Org. Chem.*, 2021, **41**, 4105–4137.
- (a) K. Y. Cheung, S. Gui, C. Deng, H. Liang, Z. Xia, Z. Liu,
 L. Chi and Q. Miao, *Chem*, 2019, 5, 838–847; (b) S. Wang,
 J. Yuan, J. Xie, Z. Lu, L. Jiang, Y. Mu, Y. Huo, Y. Tsuchido and K. Zhu, *Angew. Chem., Int. Ed.*, 2021, 60, 18443–18447.
- 10 M. Hermann, D. Wassy and B. Esser, *Angew. Chem., Int. Ed.*, 2021, **60**, 15743–15766.
- 11 (a) A. Jolly, D. Miao, M. Daigle and J.-F. Morin, Angew. Chem., Int. Ed., 2020, 59, 4624–4633; (b) J. M. Fernández-García, P. J. Evans, S. M. Rivero, I. Fernández, D. García-Fresnadillo, J. Perles, J. Casado and N. Martín, J. Am. Chem. Soc., 2018, 140, 17188–17196; (c) T. Fujikawa, D. V. Preda, Y. Segawa, K. Itami and L. T. Scott, Org. Lett., 2016, 18, 3992–3995; (d) R. Li, B. Ma, R.-Y. He, B. Zhang, Y.-K. Zhang, S.-Y. Feng and P. An, Chem.-Asian J., 2022, 17, e202101365.
- 12 (a) K. Kawasumi, Q. Zhang, Y. Segawa, L. T. Scott and K. Itami, Nat. Chem., 2013, 5, 739–744; (b) K. Kato, K. Takaba, S. Maki-Yonekura, N. Mitoma, Y. Nakanashi, T. Nashihara, T. Hata-Keyama, T. Kamada, Y. Hijikata, J. Pirillo, L. T. Scott, K. Yonekura, Y. Segawa and K. Itami, J. Am. Chem. Soc., 2021, 143, 5465–5469; (c) J. Wang, F. Gordillo Gámez, J. Marín-Beloqui, A. Diaz-Andres, X. Miao, D. Casanova, J. Casado and J. Liu, Angew. Chem., Int. Ed., 2023, 62, e202217124.
- 13 (a) M. Stępień, E. Gońka, M. Żyła and N. Sprutta, Chem. Rev., 2017, 117, 3479–3716; (b) M. Hirai, N. Tanaka, M. Sakai and S. Yamaguchi, Chem. Rev., 2019, 119, 8291–8331; (c) A. Borissov, Y. K. Maurya, L. Moshniaha, W.-S. Wong, M. Żyła-Karwowska and M. Stępień, Chem. Rev., 2022, 122, 565–788; (d) V. Barát and M. C. Stuparu, Chem.-Asian J., 2021, 16, 20–29; (e) V. Barát and M. C. Stuparu, Chem.-Eur. J., 2020, 26, 15135–15139; (f) X.-Y. Wang, X. Yao, A. Narita and K. Müllen, Acc. Chem. Res., 2019, 52, 2491–2505; (g) Y. Guo, C. Chen and X.-Y. Wang, Chin. J. Chem., 2023, 41, 1355–1373.
- 14 (a) J. Wu, W. Pisula and K. Müllen, Chem. Rev., 2007, 107, 718–747; (b) K. Müllen and J. P. Rabe, Acc. Chem. Res., 2008, 41, 511–520; (c) M. Grzybowski, K. Skonieczny, H. Butenschön and D. T. Gryko, Angew. Chem., Int. Ed., 2013, 52, 9900–9930; (d) H. Hölzel, P. Haines, R. Kaur, D. Lungerich, N. JUX and D. M. Guldi, J. Am. Chem. Soc., 2022, 144, 8977–8986.
- (a) J. Wu, A. Fechtenkötter, J. Gauss, M. D. Watson, M. Kastler, C. Fechtenkötter, M. Wagner and K. Müllen, *J. Am. Chem. Soc.*, 2004, **126**, 11311–11321; (b) J. Wu, J. Li, U. Kolb and K. Müllen, *Chem. Commun.*, 2006, 48–50.
- 16 M. A. Medel, R. Tapia, V. Blanco, D. Miguel, S. P. Morcillo and A. G. Campaña, *Angew. Chem., Int. Ed.*, 2021, **60**, 6094– 6100.
- 17 M. A. Medel, C. M. Cruz, D. Miguel, V. Blanco, S. P. Morcillo and A. G. Campaña, *Angew. Chem., Int. Ed.*, 2021, **60**, 22051– 22056.

18 (a) B. Ma, M. Xiao, P. Liu and P. An, *Synlett*, 2022, 33, 409–414; (b) B. Zhang, L. Ruan, Y.-K. Zhang, H. Zhang, R. Li and P. An, *Org. Lett.*, 2023, 25, 732–737.

Edge Article

- 19 F. S. Guziec Jr and L. J. Sanfilippo, *Tetrahedron*, 1988, 44, 6241–6285.
- 20 Deposition numbers 2238626–2238632 for compounds 5_O, 21, 23, 24_{SO}, 17_S, 18_{Se}, and 30_{HBC} contain the supplementary crystallographic data for this paper.†
- 21 P. v. R. Schleyer, C. Maerker, A. Dransfeld, H. Jiao and N. J. R. van Eikema Hommes, *J. Am. Chem. Soc.*, 1996, **118**, 6317–6318.
- 22 (a) T. Lu and F. Chen, J. Comput. Chem., 2012, 33, 580-592;
 (b) W. Humphrey, A. Dalke and K. Schulten, J. Mol. Graphics, 1996, 14, 33-38.
- (a) Y. Shen and C.-F. Chen, Chem. Rev., 2012, 112, 1463–1535;
 (b) C. Li, Y. Yang and Q. Miao, Chem.-Asian J., 2018, 13, 884–894;
 (c) J. M. Fernández-García, P. J. Evans, S. Filippone, M. Á. Herranz and N. Martín, Acc. Chem. Res., 2019, 52, 1565–1574;
 (d) T. Mori, Chem. Rev., 2021, 121, 2373–2412;
 (e) Y. Wu, L. Zhang, Q. Zhang, S.-Y. Xie and L.-S. Zheng, Org. Chem. Front., 2022, 9, 4726–4743;
 (f) P. Karak and J. Choudhury, Chem. Sci., 2022, 13, 11163–11173;
 (g) G. R. Kiel, H. M. Bergman, A. E. Samkian, N. J. Schuster, R. C. Handford, A. J. Rothenberger, R. Gómez-Bombarelli,
- C. Nuckolls and T. D. Tillet, *J. Am. Chem. Soc.*, 2022, **144**, 23421–23427; (h) Y.-F. Wu, S.-W. Ying, S.-D. Liao, L. Zhang, J.-J. Du, B.-W. Chen, H.-R. Tian, F.-F. Xie, H. Xu, S.-L. Deng, Q. Zhang, S.-Y. Xie and L. S. Zheng, *Angew. Chem., Int. Ed.*, 2022, **61**, e202204334; (i) J.-K. Li, X.-Y. Chen, W.-L. Zhao, Y.-L. Guo, Y. Zhang, X.-C. Wang, A. C.-H. Sue, X.-Y. Cao, M. Li, C.-F. Chen and X.-Y. Wang, *Angew. Chem., Int. Ed.*, 2023, **62**, e202215367.
- 24 J. M. Fernández-Garciía, P. Izquierdo-García, M. Buendía, S. Filip-pone and N. Martín, *Chem. Commun.*, 2022, 58, 2634–2645.
- 25 (a) V. Boekelheide, I. D. Reingold and M. Tuttle, J. Chem. Soc., Chem. Commun., 1973, 406–407; (b) R. S. Givens, R. J. Olsen and P. L. Wylie, J. Org. Chem., 1979, 44, 1608–1613; (c) A. Wakamiya, T. Nishinaga and K. Komatsu, J. Am. Chem. Soc., 2002, 124, 15038–15050; (d) T. Okamoto, K. Kudoh, A. Wakamiya and S. Yamaguchi, Org. Lett., 2005, 7, 5301–5304; (e) H. Kamiya, T. Kondo, T. Sakida, S. Yamaguchi and H. Shinokubo, Chem.–Eur. J., 2012, 18, 16129–16135; (f) P. R. Christensen, B. O. Patrick, E. Caron and M. O. Wolf, Angew. Chem., Int. Ed., 2013, 52, 12946–12950; (g) S. Hayakawa, K. Matsuo, H. Yamada, N. Fukui and H. Shinokubo, J. Am. Chem. Soc., 2020, 142, 11663–11668.